ORIGINAL PAPER

Role of Cerium Addition on Structural and Superconducting Properties of Bi-2212 System

**S. Bal · M. Dogruer · G. Yildirim · A. Varilci ·
C. Terzioglu · Y. Zalaoglu**

Abstract This study examines the significant changes in the structural and superconducting properties of cerium (Ce) doped Bi-2212 superconductors via X-ray diffraction analysis (XRD), scanning electron microscopy (SEM), electron dispersive X-ray (EDX), electrical resistance and transport critical current density (J_c) measurements. Ce concentration is varied from $x = 0.0$ until 0.1 in a general stoichiometry of $Bi_{1.8}Sr_{2.0}Ce_xCa_{1.1}Cu_{2.1}O_y$. Zero resistivity transition temperatures (T_c^{offset}) of the samples produced by the conventional solid-state reaction method are deduced from the dc resistivity measurements. Furthermore, the phase fractions and lattice parameters are determined from XRD measurements when the microstructure, surface morphology and element composition analyses of the samples are investigated by SEM and EDX measurements, respectively. The results show that T_c^{offset} and J_c at self-field of the samples reduced gradually with the increase in the Ce addition. Maximum T_c^{offset} of 79.7 K and J_c of 356.8 A·cm^{-2} at 77 K are obtained for pure sample as against 44.6 K and 18.7 A·cm^{-2}, respectively, for the sample doped with 0.1 wt.% Ce. According to the refinement of cell parameters done by considering the structural modulation, the Ce doping is confirmed by both an increase of the lattice parameter a and a decrease of the cell parameter c of the samples in comparison with that of the pure sample. As for SEM measurements, it is found that not only do the surface morphology and grain connectivity degrade but the grain size of the samples also decreases with the increase of the Ce addition. Moreover, EDX images indicate that the elements used for the preparation of samples distribute homogeneously and the Ce atoms enter into the crystal structure by replacing Cu atom. In addition, the variation of ΔT_c ($T_c^{\text{onset}} - T_c^{\text{offset}}$) is investigated for the presence of impurities and weak links between superconducting grains of the samples. The possible reasons for the degradation in microstructural and superconducting properties are also interpreted.

1 Introduction

With the discovery of Bi–Sr–Ca–Cu–O (BSCCO) high-temperature superconductors in 1998 [1], the interest in both the fundamental research and applications in technology and industry of these materials has been increased day by day owing to their remarkable high transition temperature, smaller power losses, high current and magnetic field carrying capacity, optical and electronic properties [2–4]. The BSCCO system obtaining a layered structure has three different phases with regard to its chemical compositions, the Bi-2201 phase ($n = 1$, $T_c \approx 20$ K), the Bi-2212 phase ($n = 2$, $T_c \approx 85$ K) and the (Bi, Pb)-2223 phase ($n = 3$, $T_c \approx 110$ K) [5]. Among the Bi-based superconductors, the double layered cuprate (Bi-2212) is superior to the others because of the fact that its oxygen stoichiometry is relatively invariant with regard to cationic addition when the samples are produced in an identical thermal environment [6–8]. Furthermore, the Bi-2212 superconductors have lesser weak link problems compared to Bi-2223 superconductors and are

S. Bal (✉) · M. Dogruer · G. Yildirim · A. Varilci · C. Terzioglu · Y. Zalaoglu
Department of Physics, Abant Izzet Baysal University, Bolu 14280, Turkey
e-mail: sevgiibal@gmail.com

Y. Zalaoglu
Department of Physics, Osmaniye Korkut Ata University, Osmaniye 80000, Turkey

suitable for the preparation of long wires and tapes with high critical current densities (J_c). However, as received the applied magnetic fields and high temperatures limit their applications due to the significant reduction in condensation energy density, strong anisotropic properties, extremely short coherence length (ξ), and large penetration depth (λ) [9, 10]. Likewise, according to the many researches [11–13], the Bi-2212 superconductors have relatively poor mechanical properties, limiting the use of these materials in most of practical applications [14]. Therefore, several methods have been studied to improve their mechanical, superconducting and flux pinning properties to make them suitable for high-temperature and magnetic field applications for years [15, 16]. Chemical doping in the superconductor materials is one of the most preferred methods [17–20] because the changes obtained by the chemical doping can be used to investigate the mechanism of high-temperature (high-T_c) superconductivity [21–24]. The critical current density and the critical temperature might be increased by the doping. The improvement of the critical current density is attributed to the enhancement of trapped flux in the superconductor material [25, 26] and single-domain structure [27, 28]; similarly, the increase in the critical temperature is associated with the enhancement of average Cu valency. Thus, the increased density of mobile holes in the CuO_2 planes [29] improves the superconductivity of the system [30]. However, sometimes the chemical doping method causes to the decrement in the number of charge carriers (either holes or electrons) in the materials and so the superconducting properties are regressed [31, 32].

The aim of the present work is to examine the effect of Ce addition on the structural and superconducting properties of Bi-2212 ceramics prepared by conventional solid-state reaction with the aid of the dc electrical resistivity, critical current density, XRD, SEM and EDX measurements. Dc electrical resistivity and critical current density for electrical and superconducting properties, XRD measurements for the phase composition and lattice parameters, SEM and EDX images for microstructure examination and element composition analyses of the samples produced are performed, respectively. The results illustrate that the Ce doping in the Bi-2212 ceramics leads to not only reduce the charge carrier numbers and grain sizes but suppress the surface morphology and grain connectivity, as well.

2 Experimental Details

In this study, samples with the nominal stoichiometry of $Bi_{1.8}Sr_{2.0}Ce_xCa_{1.1}Cu_{2.1}O_y$ ($0 \leq x \leq 0.1$) are elaborated in air by conventional solid-state reaction [33] using high purity oxides and carbonates (Alfa Aesar Co., Ltd. 99.9% purity). The accurately weighted ingredients are grounded

homogeneously by means of a grinding machine for 12 hours and calcined in a tube furnace (Protherm-Model PTF12/75/200) at 800 °C for 48 hours with a heating rate of 5 °C /min. The powders calcined are pelletized into rectangular bars with dimensions of 10 mm × 4 mm × 2 mm under a pressure of 330 MPa. The sintering process of the pellets is performed at 840 °C for 48 hours in the furnace. The heating and cooling rates of the furnace are adjusted to be 3 °C/min and 5 °C/min, respectively. The superconductor samples prepared with different Ce stoichiometry such as $x = 0$, 0.001, 0.003, 0.005, 0.01, 0.03, 0.05 and 0.1 will be herein after denoted as Ce0, Ce1, Ce2, Ce3, Ce4, Ce5, Ce6, Ce7 and Ce8, respectively.

The dc resistivity measurements are carried out on the surface of the samples by the four-probe method. Both voltage and current contacts are made with silver paint to minimize the contact resistance. The temperature (5–110 K) dependence of resistance is measured by running 5 mA dc current through the sample in the cryostat. A Keithley 220 programmable current source and a Keithley 2182A nanovoltmeter are used for the resistance measurements. Additionally, the transport critical currents of the samples in self-field are measured by home made system at 77 K in zero field using four-probe method. A programmable temperature controller (Lakeshore 340) is used for the accurate monitoring of the temperature with a stability and accuracy of ±0.01 K. The current applied parallel to the direction of the pressed surface is ramped at a constant rate (0.02 A/s) for the entire sample. The critical current (I_c) values of the samples are defined with the criterion of 1 μV/cm. The J_c values of the samples produced are calculated from the I_c and the total cross-sectional area (width of 4 mm × thickness of 2 mm). All the data obtained are recorded using the Labview computer software. Furthermore, the structural and phase analyses of the samples studied are characterized by XRD measurements by using a Rigaku multiflex diffractometer XRD with Cu K_α radiation ($\lambda = 1.5418$ Å) in the range $2\theta = 3 - 60°$ at a scan speed of 3°/min and a step increment of 0.02° at room temperature. Phase purity and lattice parameters are estimated from the XRD patterns. The accuracy in determining the lattice parameters (a and c) is ±0.0001 Å. Average sizes of the crystal of the samples prepared are also found by the Scherrer–Warren approach [34, 35]. Moreover, the surface morphology, grain connectivity and grain size of the samples are examined with the aid of a Jeol scanning electron microscope (SEM) JEOL 6390-LV, operated at 20 kV, with a resolution power of 3 nm. The elemental compositions (in the percent) and distributions (homogeneously or not) of the samples are analyzed by means of an Oxford X-ray micro-probe analysis connected to SEM. The bulk densities of the samples are also determined from their mass and geometrical dimensions to obtain the information about the structure (porosity) of the samples produced in this work.

3 Results and Discussion

3.1 Electrical Resistance Measurements

The temperature dependence of the electrical resistance (R–T) for $Bi_{1.8}Sr_{2.0}Ce_xCa_{1.1}Cu_{2.1}O_y$ with $x = 0.0$, 0.001, 0.003, 0.005, 0.01, 0.03, 0.05 and 0.1 is depicted in Fig. 1a. It is observed that all the samples show metallic behavior above the critical temperature. The normal-state resistance
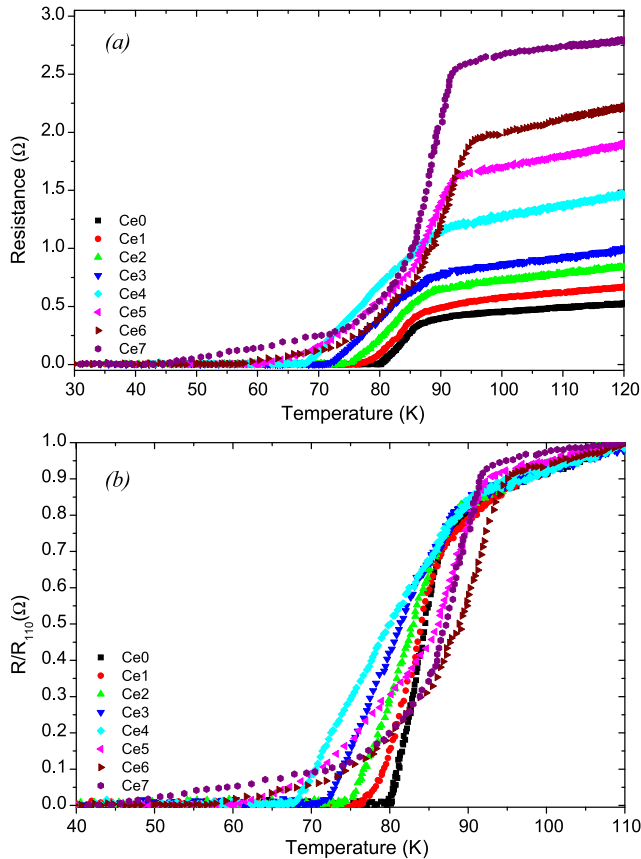

Fig. 1 (**a**) Resistance vs. temperature and (**b**) normalized resistance as a function of temperature curves for the samples

(Table 1) is found to systematically enhance with the increase in the Ce addition to a maximum (4.08 Ω) for $x = 0.1$ as against 1.21 Ω for the pure sample. When Ce^{4+} ions are doped in the system, each doping of Ce^{4+} fills one hole in the crystal. Hence, the hole concentration in the Cu–O plane of the system decreases and normal-state conductivity of the system increases. Besides, the onset critical (T_c^{onset}) and offset critical (T_c^{offset}) temperatures deduced from the normalized resistance graphs (Fig. 1b) are given in Fig. 2. As can be seen from the figure, the offset critical temperatures decrease gradually whereas the onset temperatures exhibit a wavy change with the increase of Ce-content. T_c^{offset} value is found to be about 79.7 K for the Ce0 and 44.6 K for the Ce7 sample. On the other hand, the maximum T_c^{onset} is obtained for the Ce6 sample (94.4 K) and thereafter it decreases to 91.6 K for the Ce7 sample. The variation of ΔT_c ($T_c^{onset} - T_c^{offset}$) is also shown in Fig. 3, indicating that ΔT_c increases with increase in Ce-content up to $x = 0.1$ sample. When the ΔT_c value is observed to be about 6.5 K for the undoped sample, the ΔT_c of Ce7 is obtained to be about 47.1 K (Table 1). Additionally, the broadening of the resistive transition increases as the Ce-content enhances (Fig. 1). This phenomenon indicates the presence of impurities and weak links between the superconducting grains [36], supporting the results of the SEM measurements. Consequently, the T_c^{offset} values responsible for superconductivity are observed to considerably decrease with the increase of the Ce addition.

3.2 Hole-Carrier Concentration Calculation

The hole-carrier concentrations per Cu ion, P, are calculated by means of the following relation [37]:

$$P = 0.16 - \left[\left(1 - \frac{T_c^{offset}}{T_c^{max}}\right)\bigg/82.6\right]^{1/2} \quad (5)$$

where T_c^{max} is received as 85 K for Bi-2212 phase [38] and 110 K for (Bi, Pb)-2223 phase [39] and T_c^{offset} values

Table 1 Resistivity measurement results for the samples

Samples	T_c^{onset} (K)	T_c^{offset} (K)	ΔT_c (K)	Resistance at 300 K (Ω)	Hole concentration (P)	Cell volume (nm³)	Bulk density (g/cm³)
Ce0	86.2	79.7	6.5	1.21	0.1572	0.920	5.61
Ce1	85.2	76.4	8.8	1.62	0.1250	0.917	5.59
Ce2	87.3	74.5	12.8	1.95	0.1213	0.915	5.57
Ce3	87.4	71.2	16.2	2.27	0.1156	0.912	5.51
Ce4	88.6	67.3	21.3	3.31	0.1097	0.910	5.47
Ce5	91.2	60.7	30.5	3.75	0.1011	0.907	5.44
Ce6	94.4	56.7	37.7	3.91	0.0965	0.906	5.40
Ce7	91.7	44.6	47.1	4.08	0.0841	0.904	5.38

are taken form Table 1. The P values are obtained to decrease from 0.1572 to 0.0841 and are tabulated in Table 1. The variations of hole-carrier concentrations as a function of Ce-content and superconducting transition temperature (T_c^{offset}) are also depicted in Fig. 4. It is visible that the left panel of the figure illustrates the decrement of the hole-carrier concentration with increasing Ce addition and the right panel of the figure shows the parabolic relationship between the T_c^{offset} and hole-carrier concentrations. According to these results, the Ce addition in the Bi-2212 system reduces remarkably the hole-carrier concentration, leading to the decrease in the superconducting properties of the system. Moreover, the reducing trend in the bulk density of the Ce-doped samples is observed because of the increase in the porosity of the samples prepared in this work (Table 1).
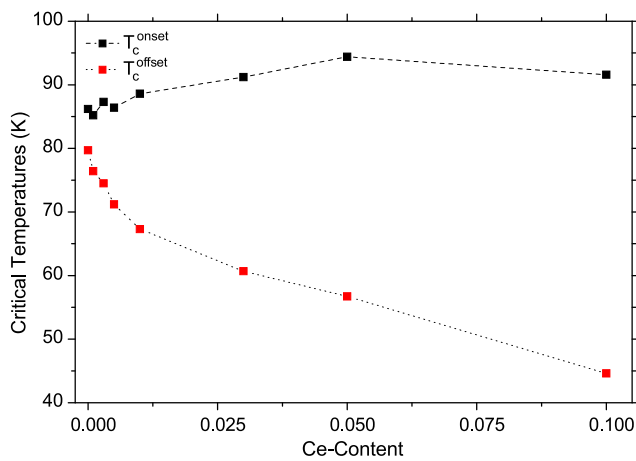
3.3 Transport Critical Current Density

Figure 5 reveals the role of the Ce-content on the self-field critical current density (J_c) of the Bi-2212 ceramics produced. The self-field J_c is found to decrease significantly for Ce-doped samples (Fig. 5a). The undoped sample indicates a J_c of 356.8 A/cm^2 that is the maximum current density in the samples prepared while the minimum J_c obtained is 18.7 A/cm^2 for $x = 0.1$ sample at 77 K (in liquid nitrogen), indicating that the J_c values of the sample decrease dramatically as the Ce-content increases (Table 2). This suppression of J_c is attributed to the increase of the weak links between the superconducting grains, porosity, secondary phases, grain boundaries resistance and de-orientation of Bi-2212 grains with the increase in the Ce addition [40, 41], supporting the results of the structural investigations. Moreover, Fig. 5b presents the parabolic variation between the

Fig. 2 T_c^{onset} and T_c^{offset} vs. Ce-content for the samples
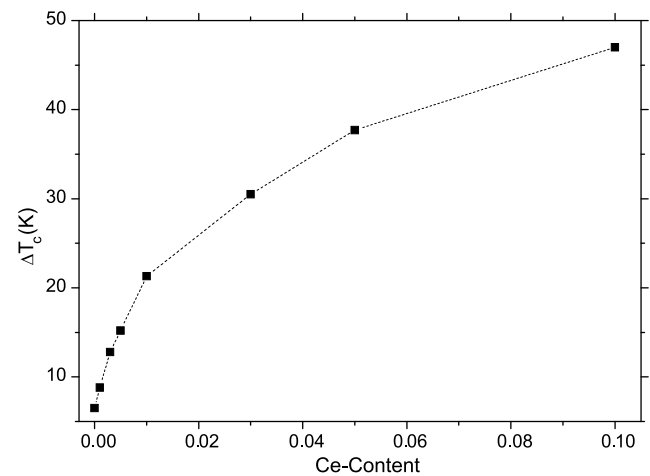

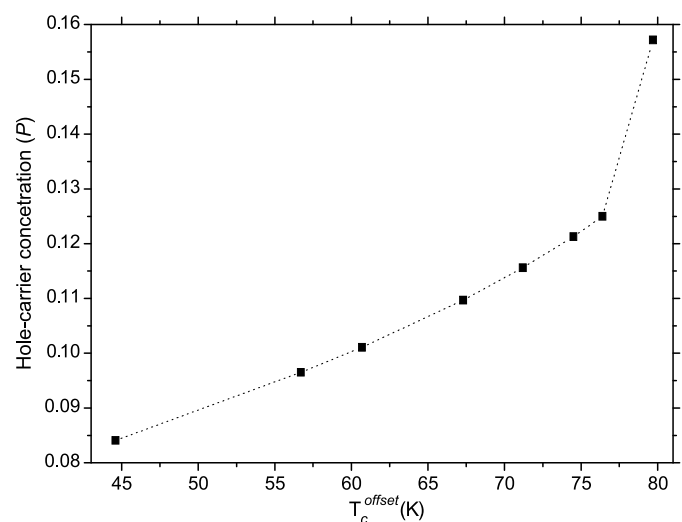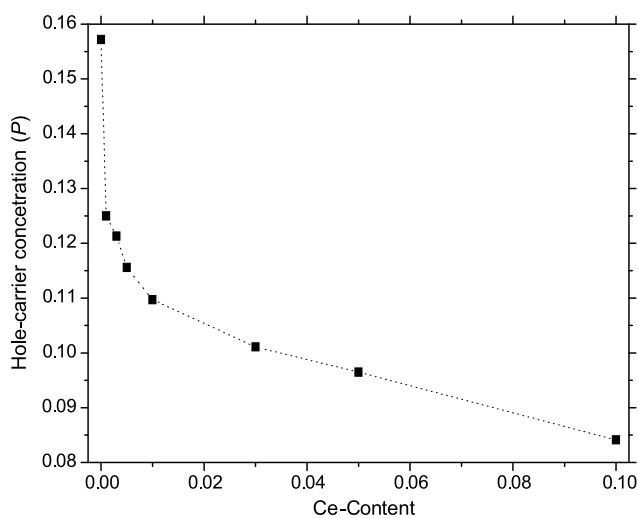**Fig. 3** Variation of T_c as a function of Ce-content for the samples

Fig. 4 *Left panel*: Variation of hole-carrier concentration vs. Ce-content and *right panel*: variation of hole-carrier concentration vs. T_c^{offset} (The *dash line* is the guide for eyes.)

superconducting transition temperatures and critical current densities of the samples. Although both the J_c and T_c values decrease with the increase in Ce addition, a sharper decline is observed in J_c values compared to the decrement of T_c values. In other words, the critical current density is found to be more sensitive to the change of Ce-content.
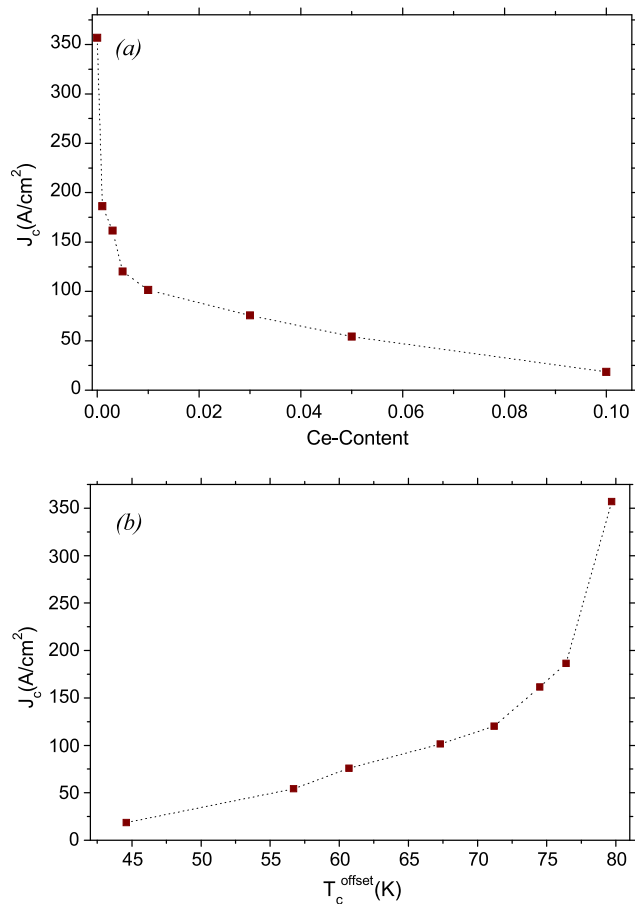

Fig. 5 (**a**) J_c vs. Ce-content graph (**b**) T_c^{offset} as a function of Ce-content for the samples

3.4 SEM Analyses

The surfaces of the samples prepared are imaged by Scanning Electron Microscopy (SEM) method. Figure 6a–h depicts the SEM pictures (taken in the secondary electron image mode) of the fractured surface of the Ce0, Ce1, Ce2, Ce3, Ce4, Ce5, Ce6 and Ce7 samples, respectively. It is clearly seen that surface morphology changes with addition of the Ce atoms in the Bi-2212 system. The grain morphology of the pure sample illustrates the clear and flaky grains with layered growth [42]. Moreover, the texturing and layered grain growth of the pure sample are found to be better compared to the doped samples. On the other hand, the grain size and texturing of the doped samples are decreased compared to the pure sample, indicating that these results are in good agreement with the Lotgering index data obtained. Using the image processing, the average grain sizes are also obtained to decrease from 540 nm to 350 nm with the Ce doping. Based on the SEM results, the surface morphology, grain connectivity and average crystallite size degrade with the increase of the Ce addition.

3.5 EDX Analyses

The quantitative values of the atomic compositions present in the Bi-2212 grains of samples are investigated by the electron dispersive X-ray (EDX). Figure 7 presents the EDX analysis for $Bi_{1.8}Sr_{2.0}Ca_{1.1}Cu_{2.1}O_y$ and $Bi_{1.8}Sr_{2.0}Ce_{0.1}Ca_{1.1}Cu_{2.1}O_y$. As seen from the figure, no difference appears between the two samples produced except for Ce peak, confirming that the Ce atoms are successfully introduced to the microstructure of the Bi-2212 phase. Moreover, Bi, Sr, Ca, Cu, O, and Ce element composition mappings taken on the surface of all the samples prepared in this work are displayed in Fig. 8a–f. It is clear that the elements used for the preparation of samples are observed to distribute homogeneously. However, the Cu compositions compared to other element compositions decrease rapidly with the increase in the Ce addition. According to the EDX results, the

Table 2 XRD and J_c measurement results for the samples

Samples	Lattice parameter a (Å)	Lattice parameter c (Å)	J_c A·cm^{-2}	Grain size (nm)	Lotgering index, F
Ce0	5.40	31.54	356.8	537	0.876
Ce1	5.41	31.41	186.3	512	0.721
Ce2	5.43	31.02	161.6	496	0.675
Ce3	5.44	30.81	120.2	472	0.654
Ce4	5.46	30.54	101.5	446	0.632
Ce5	5.47	30.31	75.4	432	0.598
Ce6	5.48	30.16	54.3	396	0.577
Ce7	5.49	30.02	18.7	356	0.529

Fig. 6 SEM micrographs of (**a**) Ce0, (**b**) Ce1, (**c**) Ce2, (**d**) Ce3, (**e**) Ce4, (**f**) Ce5, (**g**) Ce6, and (**h**) Ce7 samples
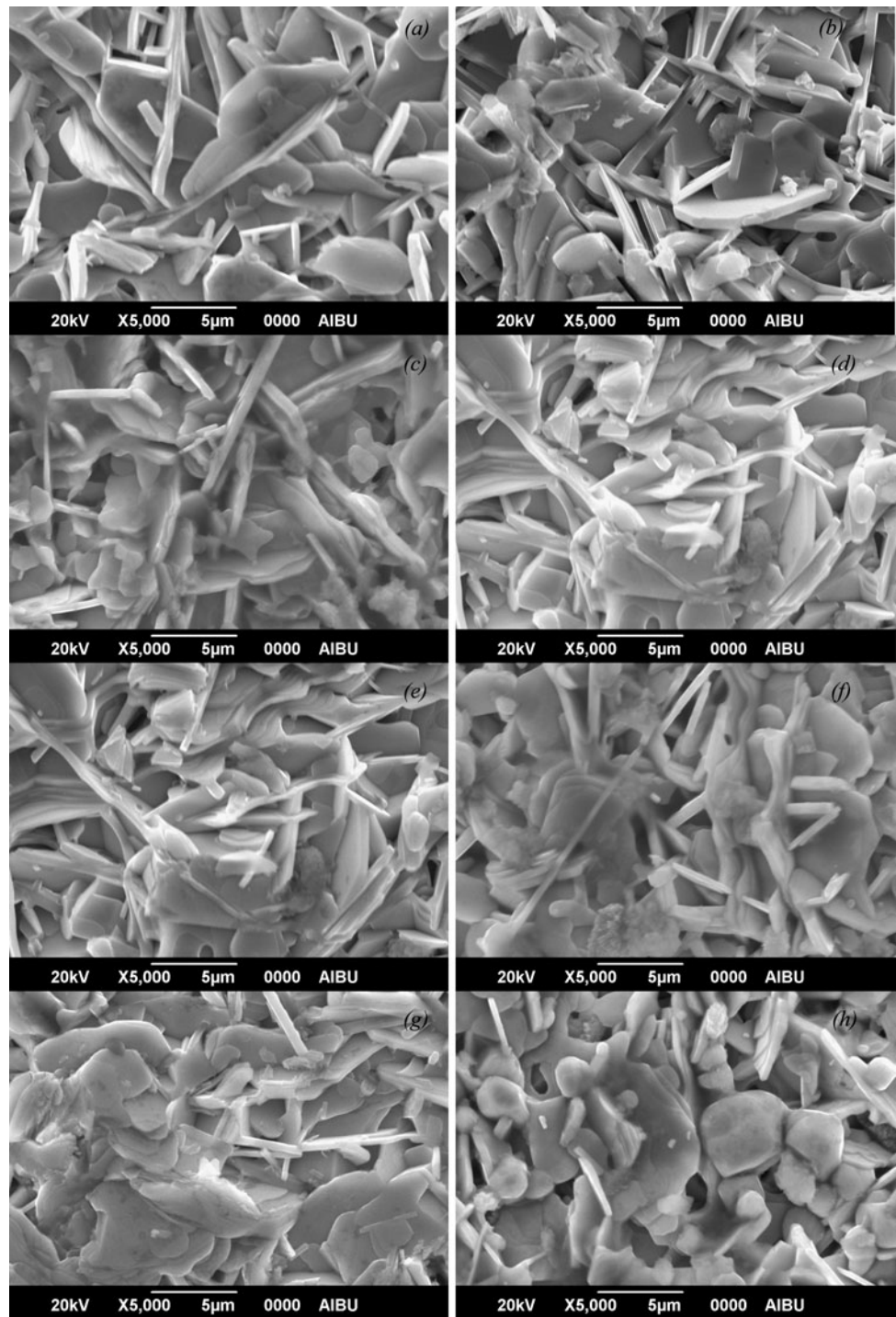
Ce atoms might enter into the crystal structure by replacing Cu atoms [43].

3.6 XRD Analyses

The XRD patterns of the samples produced are depicted in Fig. 9. The corresponding (h k l) Miller indices belonging to Bi-2212 main lines are shown in the diagrams. As

can be seen from the figure, both pure and Ce-doped samples contain the Bi-2212 phase only and all the samples studied exhibit the polycrystalline superconducting phase with less intensity of diffraction lines with increasing the Ce addition. Moreover, no secondary phase containing Ce or any other cation is observed for all the samples, indicating that Ce atoms are incorporated into the crystal structure of Bi-2212 superconductor [44–46]. The peak intensity of

the doped samples reduces regularly and other peaks such as *315*, *006* and *30̲1̲0̲* disappear completely as Ce addition increases, revealing that why the superconducting proper-

Fig. 7 EDX analysis for ... = 0.0 (**a**) and 0.1 (**b**)

ties degrade with the Ce doping in the system. Moreover, the lattice parameters *a* and *c* are calculated using the least square method through *d* values and (*h k l*) planes for tetragonal unit cell structure. The *a* and *c* parameters obtained are listed in Table 2. It is visible that a systematic expansion in the a-axis length is observed [47, 48] while a regular contraction in the c-axis length is obtained with the increase in the Ce addition [49, 50]. It is well known that the lattice parameter *a* is controlled by the length of in-plane Cu–O bond [19]. The length may be expanded or contracted with the change of the electrons into antibonding orbital. In our system this bond length is expanded because of the partial replacement of Cu^{2+} ions by Ce^{4+} ions, leading to an increase in the lattice parameter *a*, and a decrease in the lattice parameter *c*. The variation of the lattice parameters as a function of the Ce-content is also depicted in Fig. 10. As seen from the figure, there is a considerable increase in the *a* parameter and decrease in the *c* parameter. Based on these results, it might be interpreted that the Bi-2212 phase decreases while the Bi-2201 phase starts to increase with the increase of the Ce addition; however, Fig. 9 confirms that the Bi-2212 phase is dominant for all the samples studied. These findings are also ascertained by both the resistivity and SEM measurements. Furthermore, Lotgering index (*F*) is investigated to quantify the degree of *c*-axis orientation in polycrystalline ceramics produced in this work [51]. The Lotgering indices computed by means of the XRD patterns [52] are tabulated in Table 2. It is found that the texturing of Bi-2212 grains decreases monotonically with the increase of the Ce-content, supporting the SEM investigations.
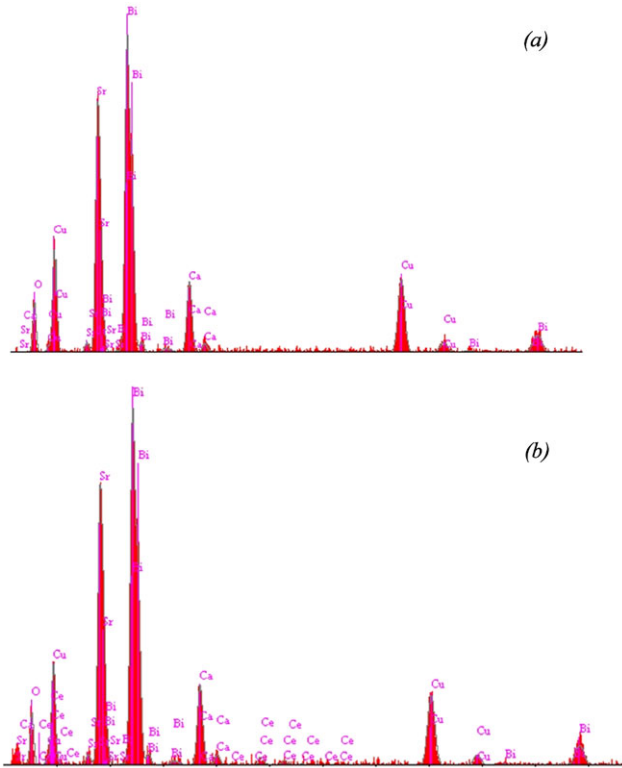
Fig. 8 EDX images of (**a**) Ce0, (**b**) Ce1, (**c**) Ce2, (**d**) Ce3, (**e**) Ce4, (**f**) Ce5, (**g**) Ce6, and (**h**) Ce7 samples

Component	Type	Line	Concentration (wt.%)
O	Calc	K_α	14.526
Ca	Calc	K_α	5.844
Cu	Calc	K_α	14.676
Sr	Calc	L_α	21.707
Bi	Calc	L_α	43.247

Component	Type	Line	Concentration (wt.%)
O	Calc	K_α	14.323
Ca	Calc	K_α	5.804
Cu	Calc	K_α	14.297
Sr	Calc	L_α	21.631
Ce	Calc	L_α	0.313
Bi	Calc	L_α	43.632

Component	Type	Line	Concentration (wt.%)
O	Calc	K_α	14.719
Ca	Calc	K_α	5.415
Cu	Calc	K_α	14.096
Sr	Calc	L_α	21.809
Ce	Calc	L_α	0.440
Bi	Calc	L_α	43.521

Fig. 8 (*Continued*)

Component	Type	Line	Concentration (wt.%)
O	Calc	K_α	14.518
Ca	Calc	K_α	5.188
Cu	Calc	K_α	13.989
Sr	Calc	L_α	21.704
Ce	Calc	L_α	0.533
Bi	Calc	L_α	44.068

Component	Type	Line	Concentration (wt.%)
O	Calc	K_α	14.908
Ca	Calc	K_α	5.123
Cu	Calc	K_α	13.056
Sr	Calc	L_α	22.270
Ce	Calc	L_α	0.672
Bi	Calc	L_α	43.971

Component	Type	Line	Concentration (wt.%)
O	Calc	K_α	14.972
Ca	Calc	K_α	4.858
Cu	Calc	K_α	12.841
Sr	Calc	L_α	22.539
Ce	Calc	L_α	0.893
Bi	Calc	L_α	43.897

Component	Type	Line	Concentration (wt.%)
O	Calc	K_α	14.842
Ca	Calc	K_α	4.150
Cu	Calc	K_α	12.283
Sr	Calc	L_α	22.832
Ce	Calc	L_α	1.406
Bi	Calc	L_α	44.222

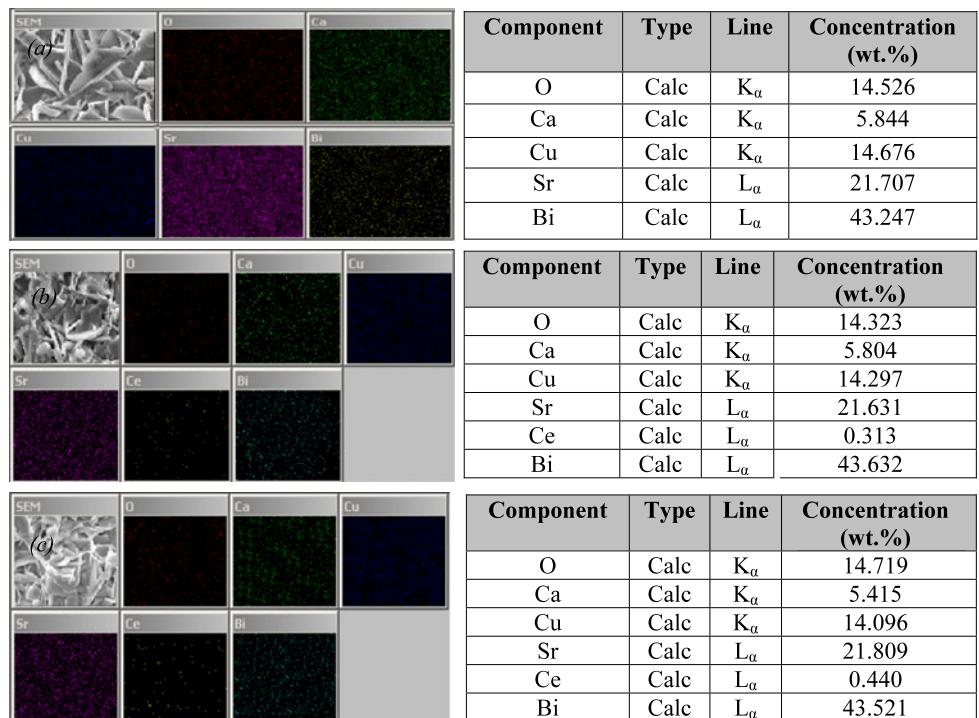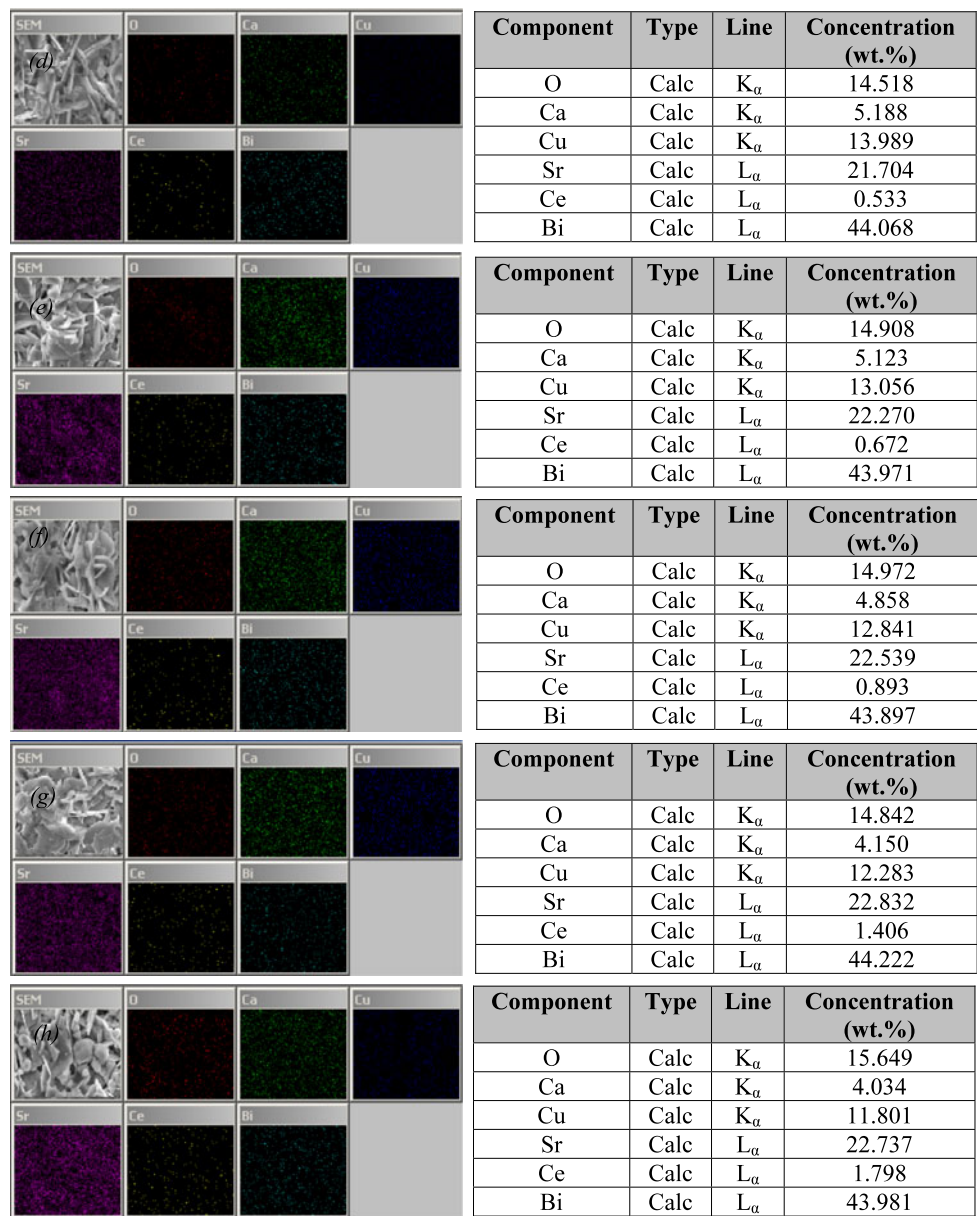| Component	Type	Line	Concentration (wt.%)
O	Calc	K_α	15.649
Ca	Calc	K_α	4.034
Cu	Calc	K_α	11.801
Sr	Calc	L_α	22.737
Ce	Calc	L_α	1.798
Bi	Calc	L_α	43.981

Additionally, the broadening nature of the XRD peaks shows that the particle sizes determined from the Scherrer–Warren equation are within the nanometer scale [53–56]. According to the equation, in broadening region the average size of a crystal is defined as;

$$d = 0.941\lambda / B \cos\theta_B \tag{3}$$

where d is the thickness of the crystal, λ is the wavelength, B is the fullwidth half maximum (FWHM) of the Bragg peak corrected using the corresponding peak in micron-sized powder and θ_B is the Bragg angle. Moreover,

$$B^2 = B_m^2 - B_s^2 \tag{4}$$

where B_s is the halfwidth of the standard material in radians. The grain size of the pure sample is calculated to be 537 nm whereas that of Ce7 sample is obtained to be about 356 nm (minimum value). Based on the calculations, the grain size of the samples studied decreases dramatically with increasing the Ce doping (Fig. 11).

4 Conclusion

In this study, the effect of Ce doping on the structural and superconducting properties of $Bi_{1.8}Sr_{2.0}Ce_xCa_{1.1}Cu_{2.1}O_y$ superconductors prepared by the conventional solid-state reaction with $x = 0, 0.001, 0.003, 0.005, 0.01, 0.03, 0.05$ and 0.1 is analyzed by means of the XRD, SEM, EDX, R–T and I–V measurements. It is found that the zero resistivity transition temperatures and transport critical current

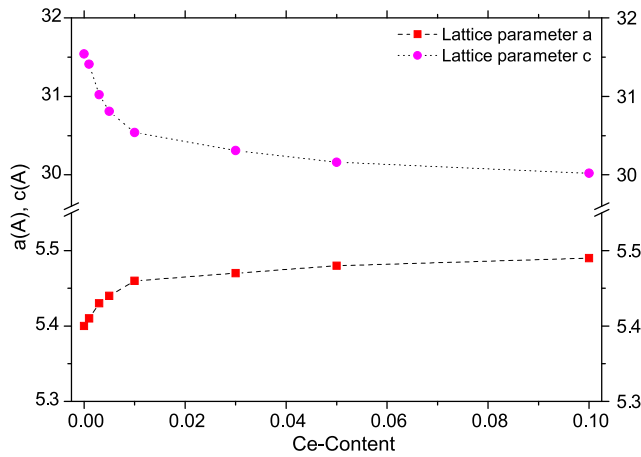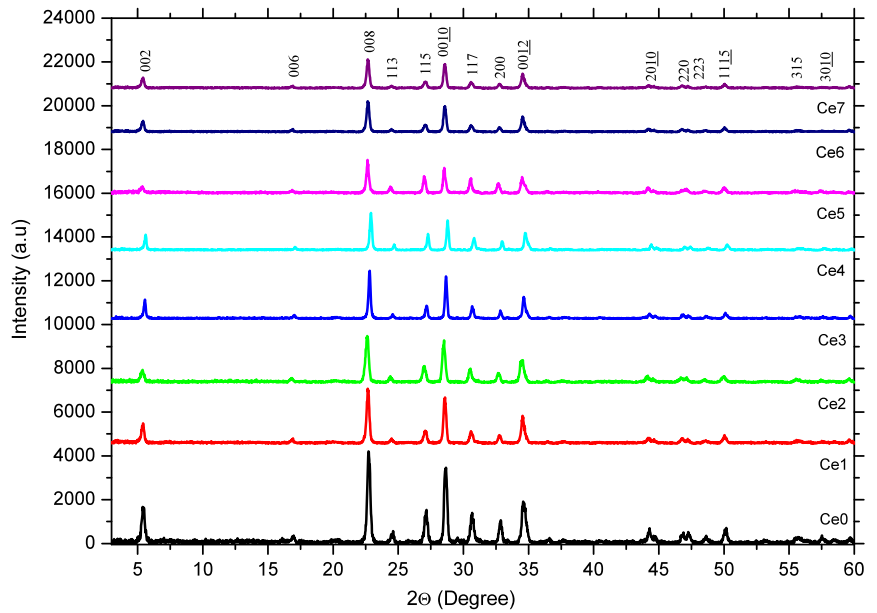**Fig. 9** XRD patterns of the Ce0, Ce1, Ce2, Ce3, Ce4, Ce5, Ce6 and Ce7 samples

Fig. 10 Variation of lattice parameter a and c as a function of Ce-content
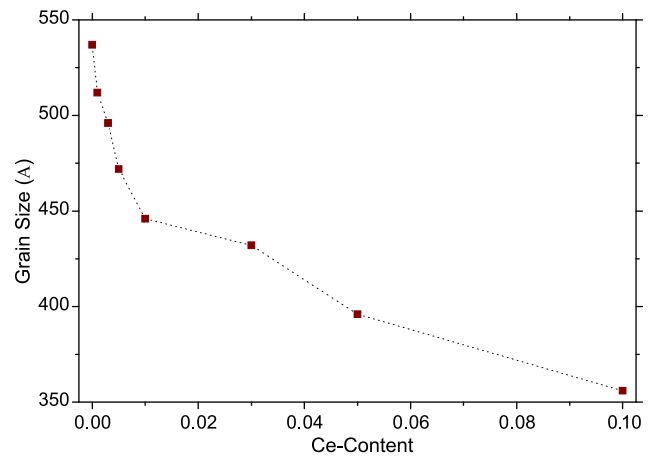
Fig. 11 Variation of grain sizes as a function of Ce-content

densities decrease from 79.7 K to 44.6 K and from 356.8 A/cm^2 to 18.7 A/cm^2, respectively, as Ce-content increases. Further, XRD investigations show that the cell parameter a increases while the c parameter decreases with increasing the Ce addition. SEM results reveal that the surface morphology and grain connectivity degrade and the grain sizes of the samples decrease from 537 nm to 356 nm with the increase of the Ce addition. As for the EDX measurements, it is seen that not only do the Cu compositions in the samples compared to other element compositions gradually decrease with the increasing the Ce doping but the elements used for the preparation of samples distribute homogeneously, as well. According to these results, the Ce atoms enter into the crystal structure by replacing Cu atoms, leading to the degradation of the structural and superconducting properties of the samples studied in this work. Besides,

the bulk densities determined from their mass and geometrical dimensions reduce slightly at a constant rate with the increase of x because of the porosity structure formation, confirming T_c and J_c values of the samples studied depend strongly on the microstructure. Based on the Lotgering index, the degree of c-axis orientation in polycrystalline ceramics produced is also found to decrease with the Ce doping.

References

1. Maeda, H., Tanaka, Y., Fukutomi, M., Asano, T.: Jpn. J. Appl. Phys. **27**, L209 (1988)
2. Runde, M.: IEEE Trans. Appl. Supercond. **5**, 813 (1995)
3. Godeke, A., Cheng, D., Dietderich, D.R., English, C.D., Felice, H., Hannaford, C.R., Prestemon, S.O., Sabbi, G., Scanlan, R.M.,

Hikichi, Y., Nishioka, J., Hasegawa, T.: IEEE Trans. Appl. Supercond. **18**, 516 (2008)

4. Miao, H., Meinesz, M., Czabai, B., Parrell, J., Hong, S.: AIP Conf. Proc. **986**, 423 (2008)

5. Mousavi Ghahfarokhi, S.E., Zargar Shoushtari, M.: Physica B **405**, 4643 (2010)

6. Awana, V.P.S., Agarwal, S.K., Ray, R., Gupta, S., Narlikar, A.V.: Physica C **43**, 191 (1992)

7. Tarason, J.M., Barboux, P., Hull, G.W., Ramesh, R., Greene, L.H., Giroud, M., Hegde, M.S., Mckinnon, W.R.: Phys. Rev. B **39**, 4316 (1989)

8. Koyama, K., Kanno, S., Noguchi, S.: Jpn. J. Appl. Phys. **29**, L53 (1990)

9. Vinu, S., Sarun, P.M., Shabna, R., Aswathy, P.M., Anooja, J.B., Syamaprasad, U.: Physica B **405**, 4355 (2010)

10. Vinu, S., Sarun, P.M., Shabna, R., Syamaprasad, U.: J. Alloys Compd. **487**, 1 (2009)

11. Yilmazlar, M., Cetinkara, H.A., Nursoy, M., Ozturk, O., Terzioglu, C.: Physica C **442**, 101 (2006)

12. Leenders, A., Ullrich, M., Freyhardt, H.C.: Physica C **279**, 173 (1997)

13. Yilmazlar, M., Ozturk, O., Gorur, O., Belenli, I., Terzioglu, C.: Supercond. Sci. Technol. **20**, 365 (2007)

14. Sedky, A.: Physica C **468**, 1041 (2008)

15. Ghazanfari, N., Kilic, A., Gencer, A., Ozkana, H.: Solid State Commun. **144**, 210 (2007)

16. Makise, T., Uchida, S., Horii, S., Shimoyama, J., Kishio, K.: Physica C **460–462**, 772 (2007)

17. Ozturk, O., Akdogan, M., Aydin, H., Yilmazlar, M., Terzioglu, C., Belenli, I.: Physica B **399**, 94 (2007)

18. Terzioglu, C., Aydin, H., Ozturk, O., Bekiroglu, E., Belenli, I.: Physica B **403**, 3354 (2008)

19. Sarun, P.M., Vinu, S., Shabna, R., Biju, A., Syamaprasad, U.: Mater. Res. Bull. **44**, 1017 (2009)

20. Sidorenko, A., Scheidt, E.W., Haider, F., Klemm, M., Horn, S., Konopko, L., Tidecks, R.: Physica B **321**, 298 (2002)

21. Eisaki, H., Kaneko, N., Feng, D., Feng, V., Damascelli, A., Mang, P.K., et al.: Phys. Rev. B **69**, 064512 (2004)

22. Kapitulnik, A., Fang, A., Howald, C., Greven, M.: J. Phys. Chem. Solids **67**, 344 (2006)

23. Tsuei, C.C., Kirtley, J.R., Hammerl, G., Mannhart, J., Raffy, H., Li, Z.Z.: J. Phys. Chem. Solids **67**, 64 (2006)

24. Fujita, K., Noda, T., Kojima, K.M., Eisaki, H., Uchida, S.: Phys. Rev. Lett. **95**(1–4), 097006 (2005)

25. Ren, Y., Weinstein, R., Liu, J., Sawh, R.P., Foster, C.: Physica C **251**, 15 (1995)

26. Ikuta, H., Mase, A., Yanagi, Y., Yoahikawa, M., Itoh, Y., Oka, T., Mizutani, U.: Supercond. Sci. Technol. **11**, 1345 (1998)

27. Xu, X.Q., Cai, Y.Q., Yang, C.X., Yao, X., Xu, S., Kortyka, A., Puzniak, R.: Supercond. Sci. Technol. **22**, 015001 (2009)

28. Xu, Y., Izumi, M., Tsuzuki, K., Zhang, Y.F., Xu, C.X., Murakami, M., Sakai, N., Hirabayashi, I.: Supercond. Sci. Technol. **22**, 095009 (2009)

29. Chevalier, B., Lepine, B., Lalerzin, A., Darriet, J., Eournau, J., Tarascon, J.M.: Mater. Sci. Eng. B **2**, 277 (1989)

30. Jayaram, B., Lanchester, P.C., Weller, M.T.: Physica C **160**, 17 (1989)

31. Guo, Y.C., Horvat, J., Liu, H.K., Dou, S.X.: Physica C **300**, 38 (1998)

32. Yildirim, G., Zalaoglu, Y., Akdogan, M., Altintas, S.P., Varilci, A., Terzioglu, C.: J. Supercond. Nov. Magn. doi:10.1007/s10948-011-1174-9

33. Yildirim, G., Akdogan, M., Altintas, S.P., Erdem, M., Terzioglu, C., Varilci, A.: Physica B **406**, 2011 (1853)

34. Cullity, B.D.: Elemt of X-ray Diffraction, 3rd edn. Addition-Wesley, Reading (2001)

35. Yucel, E., Terzioglu, C., Varilci, A., Belenli, I.: J. Mater. Sci. Mater El. (2011). doi:10.1007/s10854-010-0274-9

36. Ianculescu, A., Gartner, M., Despax, B., Bley, V., Leby, Th., Gavrila, R., Modreanu, M.: Appl. Surf. Sci. **253**, 344 (1996)

37. Azzouz, B.F., Mchirgui, A., Yangui, B., Boulesteix, C., Salem, B.M.: Physica C **356**, 83 (2001)

38. Kucukomeroglu, T., Bacaksiz, E., Terzioglu, C., Varilci, A.: Thin Solid Films **516**, 2913 (2008)

39. Persland, M.R., Tallon, J.L., Buckley, R.G., Liu, R.S., Floer, N.E.: Physica C **176**, 95 (1991)

40. Sarun, P.M., Vinu, S., Shabna, R., Biju, A., Syamaprasad, U.: Mater. Lett. **62**, 2725 (2008)

41. Abou-Aly, A.I., Mahmoud, S.A., Awad, R., Barakat, M.M.E.: J. Supercond. Nov. Magn. **23**, 1575 (2010)

42. Moodera, J.S., Meservey, R., Tkaczyk, J.E., Hao, C.X., Gibson, G.A., Tedrow, P.M.: Phys. Rev. B **37**, 619 (1988)

43. Biju, A., Syamaprasad, U., Rao, A., Xu, J.G., Sivakumar, K.M., Kuo, Y.K.: Physica C **466**, 69 (2007)

44. Vinu, S., Sarun, P.M., Biju, A., Shabna, R., Guruswamy, P., Syamaprasad, U.: Supercond. Sci. Technol. **21**, 045001 (2008)

45. Vinu, S., Sarun, P.M., Shabna, R., Biju, A., Syamaprasad, U.: Mater. Lett. **62**, 4421 (2008)

46. Shabna, R., Sarun, P.M., Vinu, S., Biju, A., Syamaprasad, U.: Supercond. Sci. Technol. **22**, 045016 (2009)

47. Wang, H., Serquis, A., Maiorov, B., Civale, L., Jia, Q.X., Arendt, P.N., Foltyn, S.R., Macmanus-Driscoll, J.L., Zhang, X.: J. Appl. Phys. **100**, 053904 (2006)

48. Sarun, P.M., Vinu, S., Shabna, R., Biju, A., Syamaprasad, U.: J. Alloys Compd. **472**, 13 (2009)

49. Shabna, R., Sarun, P.M., Vinu, S., Biju, A., Syamaprasad, U.: J. Alloys Compd. **493**, 11 (2010)

50. Biju, A., Sarun, P.M., Aloysius, R.P., Syamaprasad, U.: J. Alloys Compd. **454**, 46 (2008)

51. Lotgering, F.K.: J. Inorg. Nucl. Chem. **9**, 113 (1959)

52. Gao, W., Vander-Sande, J.B.: Supercond. Sci. Technol. **5**, 318 (1992)

53. Economy, J., Anderson, R.: Inorg. Chem. **5**, 989 (1966)

54. Shi, L., Gu, Y., Chen, L., Yang, Z., Ma, J., Qitan, Y.: Mater. Lett. **58**, 3301 (2004)

55. Budak, E., Bozkurt, C.: Physica B **405**, 4702 (2010)

56. Jiang, J.: Mater. Lett. **61**, 3239 (2007)